Ⓔ

Probabilistic Seismic-Hazard Assessment in Quito, Estimates and Uncertainties

by Céline Beauval, Hugo Yepes, Laurence Audin, Alexandra Alvarado, Jean-Mathieu Nocquet, Damiano Monelli, and Laurentiu Danciu

Online Material: National earthquake catalog for Ecuador.

INTRODUCTION

The present study is focused on estimating the probabilistic seismic hazard for the capital city of Ecuador, Quito, the population of which currently exceeds 2 million inhabitants at present. Quito is located at 2800 meters above sea level within the Interandean Depression, bounded by the equatorial line to the north, in an earthquake-prone environment (Chatelain *et al.*, 1999; Fig. 1). The city and its suburbs have developed in a piggy-back basin on the hanging wall of a reverse fault system (Fig. 2) that has been recognized as seismically active in historical, geomorphologic, geologic, and geodetic studies (Soulas *et al.*, 1991; Ego and Sebrier, 1996; Hibsch *et al.*, 1997; Egred, 2009; Champenois *et al.*, 2013; Alvarado *et al.*, 2014).

The historical record, spanning five centuries, shows that the city experienced MSK intensities (Medvedev *et al.*, 1963) in the VII–VIII range at least five times, with damages reported in churches and houses (Pino and Yepes, 1990; Egred, 2009). The most destructive earthquake was the 1859 event ($I_{\max}$ VII–VIII). Analyzing its intensity dataset, Beauval *et al.* (2010) proposed a mean magnitude M_I 7.2 (fig. 12 of their paper, M_I is an intensity magnitude equivalent to moment magnitude) and a location at an intermediate depth in the slab; a location on a shallow crustal fault cannot, however, be excluded. The 1797 Riobamba earthquake (M_I 7.6), 160 km south of Quito, produced an intensity VII in the city. A similar shaking level was experienced during another large earthquake, the 1868 Ibarra event, probably generated on the Otavalo fault located 50 km north of Quito (M_I 7.2, fig. 13 in Beauval *et al.*, 2010). Two more earthquakes, described by a sparse set of intensities and therefore difficult to characterize, could have been produced by one of the Quito fault segments. These events occurred in 1587 ($I_{\max}$ VIII, M_I 6.3–6.5, fig. 15 in Beauval *et al.*, 2010) and 1755 (observations available only in Quito, corresponding to intensity VII). In the last 150 years, no major earthquake hit Quito. The most recent significant earthquakes on the city fault system were in 1990 (M_w 5.3), and in 2014 (12 August, M_w 5.1); in both cases three inhabitants were killed in the northern suburb of Pomasqui (location indicated in Fig. 2). In an attempt to extend the observation time window, Hibsch *et al.* (1997) analyzed earthquake-induced deformation phenomena in lacustrine sediments in the northern part of the Quito basin. They studied approximately a 1500-year time span prior to the historical record. One major event was identified (intensity evaluated to X, greater than the maximum intensity in the historical record) between the tenth and the sixteenth centuries, which they believed could have ruptured the entire Quito fault reaching a magnitude 6.5–7.0. This is the unique evidence for such a large earthquake on the fault system. More recently, the seismic potential of the Quito fault was confirmed on the basis of observations covering a much shorter time window. Analyzing Global Positioning System (GPS) measurements at sites with 10–15 years of recordings, east–west horizontal shortening rates were estimated in the 4.3–5.3 mm/yr range across this blind thrust (Alvarado *et al.*, 2014).

Since 2007, a joint collaboration between France and Ecuador has been in place to prepare all the necessary inputs for computing PSH for Ecuador. The research laboratories involved are the Geophysical Institute (IG) in Quito, ISTerre in Grenoble, and Géoazur in Nice. The IG has a governmental mandate to monitor earthquakes and provide national seismic-hazard estimations. PSH maps are the basis for establishing seismic building codes. A PSH assessment requires a seismicity model, a description of the probability of occurrence of future earthquakes, and a ground-motion prediction equation (GMPE), which gives the probability of occurrence of accelerations as a function of magnitude and distance. As the Ecuadorian strong-motion network is very young, GMPEs established elsewhere in the world must be imported.

By analyzing seismicity distribution, active faults and plate margins, as well as geodetic measurements, Alvarado (2012, Fig. 3) subdivided the region into seismic sources. This seismotectonic zoning is the one used in our 2011 PSH calculations that we provided to the Ecuadorian committee in charge of establishing the new Ecuadorian building code (MIDUVI-CCQ, 2011). Beauval *et al.* (2010, 2013) created a unified and homogeneous earthquake catalog for Ecuador and borders covering five centuries and integrating instrumental and historical events (Ⓔ see Tables S1 and S2, available in the

 doi: 10.1785/0220140036

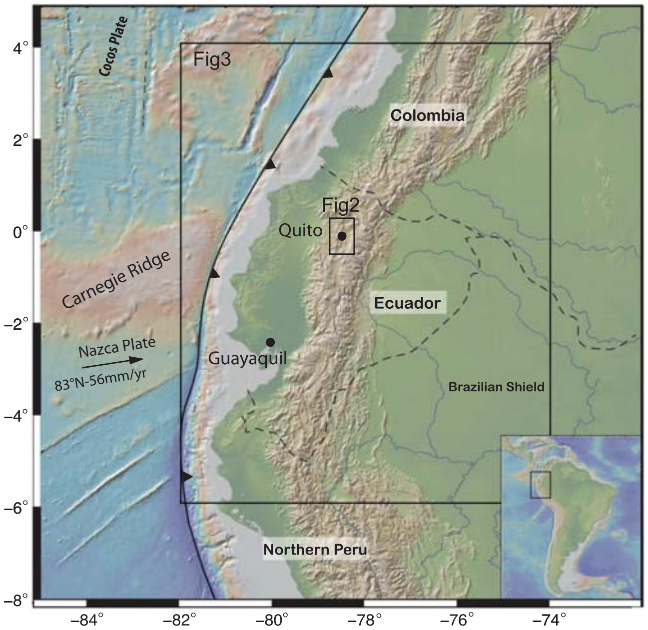

▲ **Figure 1.** Regional map of the study, rectangles define the areas displayed in Figures 2 and 3. Inset shows South America with the plotting region marked.

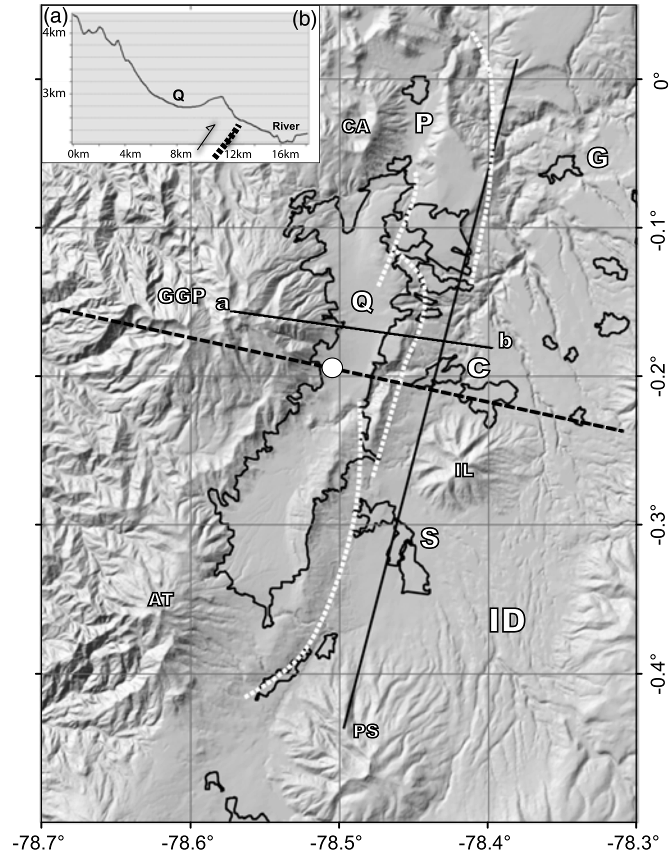

▲ **Figure 2.** Geomorphology and tectonic setting of the Quito basin. The city has grown on a 50 km long piggy-back basin generated by the permanent activity of the Quito reverse fault dipping west. Northeast–southwest-trending hills bordering Quito to the east: folds are produced by the thrust movement of the blind fault. White dashed lines: detailed fault segments identified in Alvarado *et al.* (2014). North–south black segment indicates the projection of the Quito fault top edge to the surface (simplified model, dip 50°). Altitude difference between the basin and the Interandean Depression (ID) is 600 m (see the a–b cross section, inset, vertical axis denotes altitude above sea level in kilometers). Contours indicate city and neighboring suburbs (Q, Quito; P, Pomasqui; S, Sangolqui; G, Guayllabamba; C, Cumbaya). Neighboring volcanoes: GGP, Pichincha; AT, Atacazo; PS, Pasochoa; IL, Ilaló; CA, Casitagua. White dot indicates rock site considered in the study; dashed black segment indicates profile studied in Figure 10.

electronic supplement to this paper). The present study proposes to estimate PSH in Quito based on the Alvarado (2012) zoning coupled with the newly published earthquake catalog. The OpenQuake engine is used for all PSH calculations (Global Earthquake Model, www.globalquakemodel.org/ (last accessed October 2014); Crowley *et al.*, 2013; Pagani *et al.*, 2014). We focus on hazard estimate at 475 years return period, corresponding to a 10% probability of exceedance over 50 years. Our approach is first to identify the controlling parameters and then to evaluate the uncertainties on these parameters and the corresponding impact on the hazard levels.

PROBABILISTIC SEISMIC HAZARD IN QUITO: THE HOST ZONE IS CONTROLLING THE HAZARD

The territory of Ecuador has been subdivided into seismic sources, producing a seismotectonic model with 26 source zones. The criteria used for deriving this model are described in Alvarado (2012). Crustal sources enclose fault systems or zones of diffuse seismicity. Recurrence curves are modeled based on the observed seismicity rates using the earthquake catalog (Ⓔ see Tables S1 and S2) and the time windows of completeness published in Beauval *et al.* (2013) and reported in Table 1. Different complete time periods have been determined for shallow earthquakes occurring in the Cordillera and for subduction earthquakes. For example, all earthquakes with magnitudes $M_w \geq 4.5$ are considered complete since 1963, whereas earthquakes with magnitudes $M_w \geq 6.0$ are complete since 1860 in the Cordillera and since 1900 for the plate margins (interface events) and at depth (inslab events). Recurrence rates are estimated for magnitudes 4.5 and above, together with the *b*-value (applying Weichert, 1980; see, e.g., Beauval and Scotti, 2003). All crustal sources are modeled as a real zones, with seismicity rates distributed over depth according to the observed depth distribution of instrumental earthquakes in each zone (up to 35 km in the Cordillera). Based on selected earthquake focal mechanisms and tectonic analysis (Alvarado, 2012), predominant focal mechanisms are identified and further taken into account in the prediction of ground motions. The subduction interfaces are modeled as dipping fault planes, the segmentation along the trench relies on the rupture zone estimated from past megaearthquakes (Esmeraldas zone,

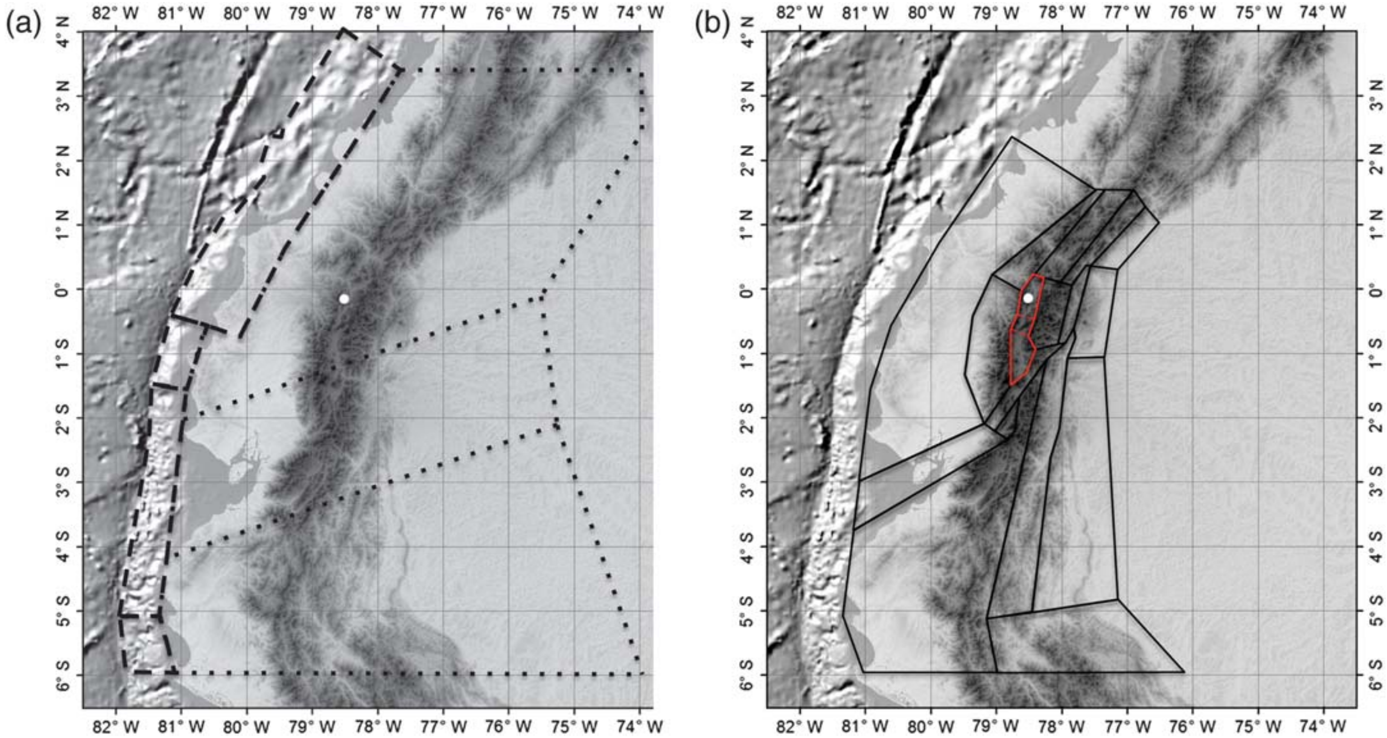

▲ **Figure 3.** Seismotectonic sources for probabilistic seismic-hazard assessment in Ecuador (Alvarado, 2012). (a) Interface subduction planes (dashed lines) and inslab volumes (dotted lines); (b) shallow crustal source zones (continuous black lines); Quito, Machachi, and Latacunga source zones highlighted in red (see Fig. 5). White dot: the rock site in Quito considered in the study.

corresponding to the rupture plane of the 1906 M_w 8.8 event) or on the seismicity pattern observed along the interface zone. The subduction inslab zones are modeled as volumes, with seismicity distributed between 35 and 200 km. Maximum magnitudes in each source zones are based on the maximum length of fault segments identified as active using the magnitude–length equations published in Leonard (2010) and Strasser *et al.* (2010). We checked that these magnitudes inferred from active tectonics are always higher or equal to the maximum historical magnitudes recorded in the zones.

The first hazard calculations identify the contributions to the hazard in Quito of crustal sources, inslab volumes, and interface planes. Calculations are performed for a rock site located in Quito (coordinates −78.51 in longitude and −0.2 in latitude, Figs. 2 and 3), applying the GMPE for a V_{S30} of 760 m/s (shear-wave velocity in the top 30 m). To begin with, the GMPE Zhao *et al.* (2006) is used for the three tectonic regimes to predict the ground motions produced by earthquakes. Zhao *et al.* (2006) is based on the rupture distance (closest distance to the fault plane, R_{rup}). The minimum magnitude considered in the probabilistic calculation is M_w 5.0; Gaussian distributions predicted by GMPEs are truncated at $\pm 3\sigma$. Hazard curves are calculated taking into account all source zones and then considering separately the crustal source zones, the inslab sources, and the interface sources (Fig. 4a, for peak ground acceleration [PGA]). Using the GMPE Zhao *et al.* (2006) for the three tectonic regimes, an acceleration of 0.41g is obtained at 475 years, when either all sources or only the crustal host zone is considered. These results show that, for a site on rock (V_{S30}760 m/s), there is only one source zone—the host crustal zone—that contributes significantly to the seismic hazard in Quito (PGA) for 475 years return period. The same calculations, using other GMPEs (for crustal sources: Boore and Atkinson, 2008; Akkar and Bommer, 2010, both based on Joyner and Boore distance R_{JB}; for subduction sources: Youngs *et al.*, 1997), indicate that the host source always controls the hazard in Quito at 475 years. This result is also valid for spectral frequencies over the 0.1–1 s range. The uniform hazard spectra displayed in Figure 4b show that the spectral accelerations at 475 years based on the full seismicity

Table 1
Completeness Time Windows Used in the Modeling of Earthquake Recurrence in the Source Zones

Magnitude interval	4.0–4.5	4.5–5.0	5.0–5.5	5.5–6.0	6.0–6.5	6.5–7.0	7.0–7.5
Time period of completeness: crustal sources	1997	1963	1957	1920	1860	1860	1587
Time period of completeness: subduction sources	1997	1963	1963	1963	1900	1900	1900

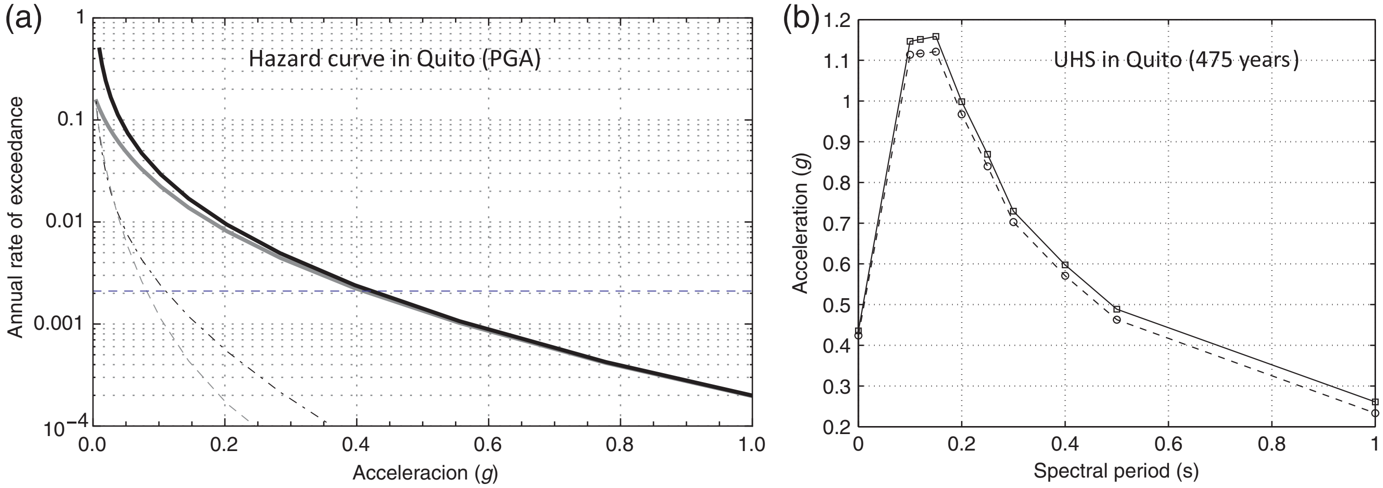

▲ **Figure 4.** (a) Hazard curves for a site located at rock in Quito (peak ground acceleration [PGA]). Total hazard curve including contributions from all sources (black solid curve), hazard curves including only the contribution from the crustal host zone (solid gray curve), the interface sources (dotted dashed curve), and the inslab sources (dashed curve). (b) Contribution of the host crustal zone to the total hazard in Quito: Uniform Hazard Spectrum (UHS) including contributions from all source zones (solid line) and UHS including only the contribution from the host zone (dashed line). Zhao *et al.* (2006) model used for the three source zone types.

model are very close to the accelerations relying only on the host zone contribution.

For the hazard at 475 years return period in Quito (0.41g for the PGA), the interface contribution is negligible with respect to the contribution of the crustal host zone. Nonetheless, considering the interface sources alone, an acceleration of 0.12g is obtained in Quito at 475 years return period (Fig. 4a). The interface contributing is the Esmeraldas zone, modeled as a dipping plane (20°) between 4 and 44 km depth, extending over the rupture area of the 1906 event (from latitude −0.5° to +4°, approximately 500 km long, Fig. 3a), with maximum magnitude 8.8 (M_w). The Gutenberg–Richter recurrence curve established from the seismic catalog predicts one earthquake with magnitude ≥ 7.0 on average every 25 years in this source zone, and one earthquake with magnitude ≥ 8.0 on average every 110 years. However, this interface is located at 200 km from Quito, and its contribution to the annual exceedance rate for an acceleration of 0.41g is negligible (calculations at rock).

VARIABILITY OF THE UNIFORM HAZARD SPECTRUM AT 475 YEARS

Host Zone: Frequency–Magnitude Distributions

We now focus on the host zone controlling the seismic hazard in Quito. The characterization of the Quito reverse fault system has improved significantly with the use of Interferometric Synthetic Aperture Radar (InSAR) by Champenois *et al.* (2013) and the use of geomorphology, tectonics, and GPS by Alvarado *et al.* (2014). However, the information available does not yet permit to propose a recurrence model for each fault segment. Rather than considering individual segments in the PSH calculations, an areal seismic source has been delineated enclosing the whole reverse fault system (Figs. 3b and 5a, c). The prolongation of the Quito fault system to the south is the reverse Latacunga system (see e.g., fig. 16 in Beauval *et al.*, 2010, named Poalo-Saquisilí-Yambo fault), both dipping to the west. Between these systems (between latitudes −0.4° and −0.7°), no fault trace has been clearly identified, although historical earthquakes, for example in 1923, have occurred there (Beauval *et al.*, 2013). Following Alvarado (2012), two options are proposed for delineating the source zone enclosing Quito (host zone). The first one (option S1, Fig. 5a) is a large area enclosing both fault systems, extending from latitude −1.15° to +0.5° (Quito–Latacunga zone). This option has been used in the previous calculations (see Probabilistic Seismic Hazard in Quito: The Host Zone is Controlling the Hazard section). As Alvarado *et al.* (2014) note, the north–south-trending Quito and Latacunga reverse faulting systems are geodynamically similar because they form the western boundary of the "Quito–Latacunga microblock" (~150 km long). The fault systems located to the north and to the south of this microblock trend northeast–southwest and have right-lateral strike-slip mechanism. The microblock is characterized by discontinuous Quaternary folds and piggy-back basins related to blind thrusts with evidences of tilted young volcanoclastic deposits (Lavenu *et al.*, 1995; Alvarado *et al.*, 2014). Available focal mechanisms for $M_w \geq 5.0$ earthquakes suggest a common present day behavior along strike. The second option isolates each fault system and divides the large zone into three smaller ones (Quito, Machachi, and Latacunga zones, Fig. 5b,c). As the Latacunga source zone contains more earthquakes than the Quito source zone, the hazard evaluated in Quito will be higher for the large host zone option (S1) than for the small Quito host zone option (S2).

The recurrence curve corresponding to the Quito zone relies on very few events (Fig. 6b). Seven events with magnitudes

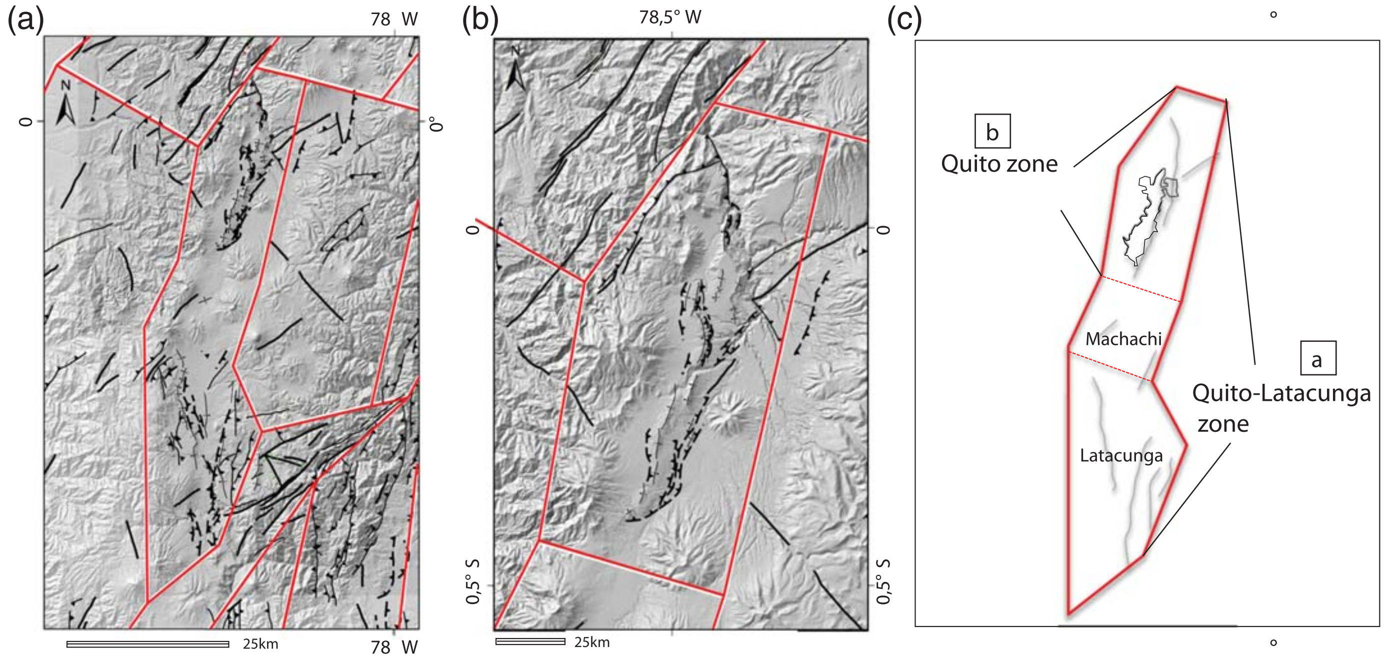

▲ **Figure 5.** Two crustal host zone definitions. (a) The Quito–Latacunga zone enclosing both the Quito fault system and the Latacunga reverse fault system (Poalo-Saquisili-Yambo fault system in Beauval *et al.*, 2010), option S1. (b) The Quito zone enclosing the Quito reverse fault system (option S2). (c) Scheme displaying the two options for the crustal host zone. See Figure 3b for the location of these zones in a regional perspective.

$M_w \geq 4.5$ belong to the source zone; the greatest magnitudes are M_I 5.8 (10 August 1938, Sangolqui event, Beauval *et al.*, 2010) and M_I 6.4 (31 August 1587, Guayllabamba event, Beauval *et al.*, 2010). Six events fall inside the completeness time windows ($4.5 \leq M_w \leq 5.8$). One option is to work with the rate and b-value inferred from this scarce catalog ($b = 0.81$). Around 0.11/year events with $M_w \geq 4.5$ occur within this source zone, equivalent to 1 event $M_w \geq 4.5$ every 9 years. Another option is

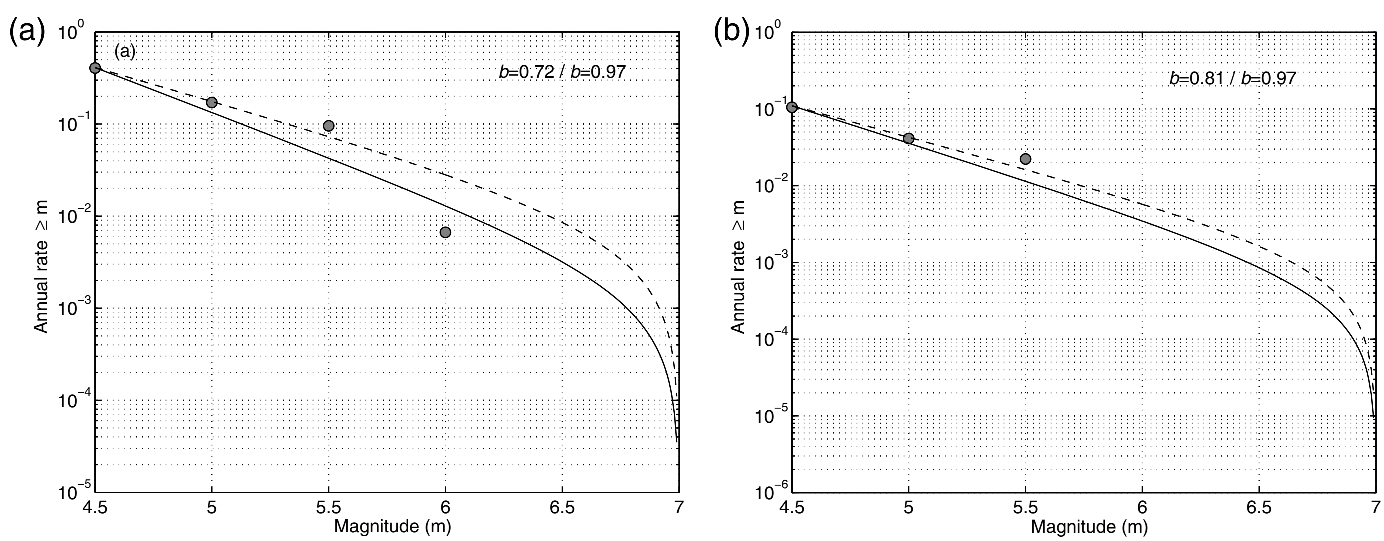

▲ **Figure 6.** Recurrence curves for the host zone, superimposed to the observed rates (completeness time windows in Table 1). (a) The host zone is the Quito–Latacunga zone enclosing both the Quito and the Latacunga fault system (see Fig. 5a): dashed line, recurrence based on 27 events with $M_w \geq 4.5$ and depth lower than 35 km, $a = 2.42$ and $b = 0.72$ (Gutenberg–Richter, 1944 parameters); solid line, recurrence curve based on the observed rate for M_w 4.5+ and on the b-value from the Cordillera region. (b) The host zone is the Quito zone enclosing only the Quito fault system (S2, Fig. 5b): dashed line, recurrence curve based on 7 events with $M_w \geq 4.5$ and depth lower than 35 km, $a = 2.69$ and $b = 0.81$; solid line, recurrence curve based on the observed rate for M_w 4.5+ and on the b-value from the Cordillera region.

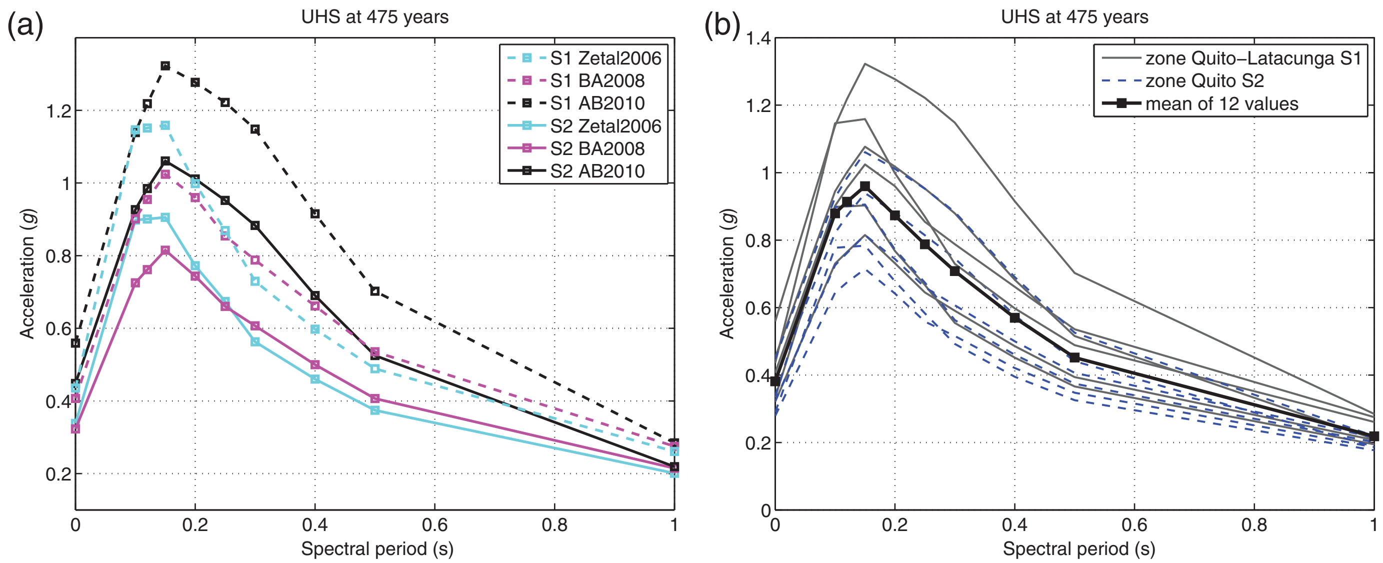

▲ **Figure 7.** Uniform hazard spectra for a rock site in Quito, at 475 years return period. (a) Testing two geometries for the host source zone, S1 and S2 (see Variability of the Uniform Hazard Spectrum (UHS) section), and three ground-motion prediction equations (GMPEs) for crustal events (AB2010: Akkar and Bommer, 2010; BA2008: Boore and Atkinson, 2008; Zetal2006: Zhao *et al.*, 2006). (b) UHS resulting from the final logic tree including two geometries for the host zone, two optional *b*-values, and three GMPEs. Black indicates host source zone option S1 and blue indicates host source zone option S2. All source zones are taken into account in the calculations (crustal, interface, inslab), although interface/inslab contributions are negligible at this return period.

to use only the observed rate for magnitudes $M_w \geq 4.5$ and associate this rate with the more robust *b*-value calculated considering the whole Cordillera ($b = 0.97$, Beauval *et al.*, 2013). As for the larger Quito–Latacunga source zone, 27 events with $M_w \geq 4.5$ belong to this spatial zone. The recurrence parameters are retrieved from a catalog of 24 events falling in the completeness time windows (yielding $b = 0.72$, Fig. 6a). The earthquake catalog of this zone includes several events $M_w \geq 5.5$, which are linked to the Latacunga fault system, mostly in the twentieth century (1736, 1944, 1960, 1962, 1976, and 1996), with maximum observed magnitude 6.1 in 1757 (Beauval *et al.*, 2010, 2013). Two further events in 1923 (M_{IC} 5.8–6.5) and 1929 (Murco event, M_{IC} 5.9) fall in this zone, in the area where no fault trace has been evidenced. The Gutenberg–Richter model predicts 0.41 events per year with $M_w \geq 4.5$ within this source zone, corresponding to 1 event every ~2.5 years. These recurrence curves need to be bounded in the upper range. All the segments of the Quito fault system breaking at once would produce an earthquake with approximately 50 km subsurface length rupture (Fig. 2). Applying the Wells and Coppersmith (1994) magnitude–length relationship for this fault gives a magnitude ~7.0: $\mathbf{M} = 4.49 + 1.49 \times \log_{10}(L)$ with $L = 50$ km. The relationship from Leonard (2010) gives similar results.

Variability of the Uniform Hazard Spectrum (UHS)

To begin with, three equations are selected to explore the epistemic uncertainty of the ground-motion predictions from crustal earthquakes: Zhao *et al.* (2006), established from Japanese data; Akkar and Bommer (2010), based on European and Middle East data; and Boore and Atkinson (2008), using western United States strong motions. Tested against diverse strong-motion datasets, these equations proved to be robust and stable models over the full frequency range (e.g., Delavaud *et al.*, 2012; Beauval, Tasan, *et al.*, 2012). As inslab and interface sources have a negligible contribution to the hazard at 475 years, only one GMPE is considered for these sources, namely, Zhao *et al.* (2006), which was identified among best-fitting subduction models for South America in Arango *et al.* (2012) and Beauval, Cotton, *et al.* (2012). We confirmed that the present results are similar if Youngs *et al.* (1997) is used.

We estimated PSH using two definitions for the host zone contour (S1 or S2, seismic rates for **M** 4.5+ and *b*-values based on the zone dataset), and the three selected GMPEs. The six combinations of source zones and GMPEs result in six uniform hazard spectra at 475 years (Fig. 7a). As expected, using the zoning S2 provides lower hazard estimates in Quito than when using the zoning S1. For the PGA, results vary between $0.32g$ and $0.55g$, depending on the zonation used and on the GMPE selected. Based on Akkar and Bommer (2010), the PGA increases from $0.46g$ (S2) to $0.55g$ (S1); whereas in the case of Boore and Atkinson (2008), the PGA increases from $0.32g$ to $0.41g$. Keeping the zoning fixed (S2), the PGA increases from $0.32g$ to $0.46g$ if using Akkar and Bommer (2010) instead of Boore and Atkinson (2008) ($0.41g$–$0.55g$ in the case of S1). These calculations show that the hazard in Quito at 475 years is controlled both by the definition of the areal host zone (~20%–30% variability at the PGA, ~30%–35% variability at 0.5 s) and by the choice of the GMPE selected for this zone (~35%–45% variability at the PGA, ~30%–35% variability at 0.5 s), for all spectral periods up to 0.5 s (Fig. 7a). At the spectral period of 1 s, the impact of the choice of the host zone is much higher than the impact of the GMPE choice.

The recurrence model in the source zone S2 is not well constrained. The rate for events with $M_w \geq 4.5$ and the b-value, used for extrapolating this rate to higher magnitudes, rely on very few events (see Host Zone: Frequency–Magnitude Distributions section). To take into account the uncertainty on the recurrence model, two more recurrence models are included in the analysis. Gutenberg–Richter curves based on the rates of M ≥4.5 coupled with the well-constrained 0.97 b-value of the Sierra region (Fig. 6) are now considered. This b-value is larger than the b-values estimated from the zone dataset, producing lower seismic rates over the magnitude range [4.5–7.0]. The uncertainty in the predicted recurrence of earthquakes with magnitudes 6 and larger is significant. The mean recurrence time in the Quito–Latacunga zone S1 varies between 33 and 90 years, depending on the b-value selected. In the case of the smaller Quito zone S2, the recurrence time for an earthquake **M** ≥ 6.0 varies between 166 and 285 years. Results for this simple logic tree, obtained from the combination of four seismicity models for the host zone and three crustal GMPEs, are displayed in Figure 7b. The PGA in Quito at 475 years varies between 0.28g and 0.55g, with the mean value around 0.39g. At 0.2 s (5 Hz), accelerations vary between 0.63g and 1.28g, with a mean around 0.88g, whereas at 0.5 s (2 Hz), accelerations vary between 0.32g and 0.7g, with a mean value around 0.45g.

Frequency–Magnitude Distributions Based on the Slip Rate and Corresponding Hazard

Recent development of geodetic (GPS) networks in Ecuador provided the first present-day estimates of crustal deformation and slip rates on major faults (Nocquet *et al.*, 2014). In the Quito area, GPS results spanning a period of ~15 years show a horizontal shortening rate at ~4 mm/yr between sites located west and east of the Quito fault system (Alvarado *et al.*, 2014). Alvarado *et al.* (2014) further show that GPS data are well modeled by a single fault with an associated slip rate ranging from 4.3 to 5.3 mm/year. Moreover, a sharp velocity gradient observed across the Quito fault system indicates that only a fraction of the fault plane is presently accumulating elastic stress, available for future earthquakes. More precisely, Alvarado *et al.* (2014) found that the depth over which elastic stress is presently accumulated is in the range of 3–7 km.

The average slip-rate estimates can be used to propose alternative earthquake occurrence relations independent of the earthquake catalog (see e.g., Anderson and Luco, 1983; Youngs and Coppersmith, 1985; Bungum, 2007). Under the assumption that deformation remains steady in time, geodetically derived fault slip rates can be used to propose earthquake frequency–magnitude distributions consistent with the annual rate of moment deficit accumulation. The Quito zone is an area of approximately 70 km × 40 km, which encloses the Quito fault. Most of the seismicity in the zone is related to the Quito fault system. This fault system is composed of several blind thrust segments, the exact geometries and extensions in depth of which are yet to be defined (Alvarado *et al.*, 2014). For the purpose of the calculation, a simplified geometry is considered. The fault is modeled as a single segment of 50 km (subsurface length, latitudes 0.0275° to −0.423° and longitudes −78.385° to −78.50°, Fig. 2).

Although the fault slip rate constrains the seismic moment rate to be released on the fault, a model is required to distribute it through earthquakes of various magnitudes. Anderson and Luco (1983) propose a frequency–magnitude distribution constrained by the slip rate, the b-value, and the maximum magnitude M_{max} on the fault. They have reviewed several forms of recurrence relationships that have been developed using slip-rate constraints. Following the work achieved in the SHARE project (Woessner *et al.*, 2012), the model number 2 providing the activity rate N_2 is selected (table 3 in Anderson and Luco, 1983; equation 7 in Bungum, 2007). The cumulative number of earthquakes with magnitude greater than M is modeled by an exponential function truncated at M_{max}. The density function decreases continuously to zero as M approaches M_{max}. The number of earthquakes N above magnitude 5.0 (M_{min} in the PSH calculation) is calculated as follows:

$$N(m \geq 5.0) = \frac{d\ln(10) - b\ln(10)}{b\ln(10)} \frac{S}{\beta}\left[e^{b\ln(10)\times(M_{max}-M)} - 1\right] \times e^{-\frac{d\ln(10)M_{max}}{2}},$$

in which

$$\beta = \sqrt{\frac{\alpha M_0(0)}{\mu W}}; \qquad \alpha = \frac{D}{L};$$

$$\log M_0 = c + dM(c = 160.5, d = 1.5)$$

S is the slip rate. The b-value is assumed equal to the b-value from the Quito zone dataset (0.81, Fig. 6b). The well-known log–linear relation between the seismic moment M_0 and moment magnitude is used (Kanamori and Anderson, 1975). The rigidity modulus is fixed to 3.0×10^{11} dyn/cm^2. The parameter α is the ratio of the average displacement D in the largest earthquake rupturing the total width to the fault length L. This parameter bears large uncertainties. Considering an average displacement from 1 to 2m (earthquake with magnitude ~7.0, Wells and Coppersmith, 1994), and assuming a length equal to 50 km, yields the range 2×10^{-5} to 4×10^{-5} for α. These values are in accordance with $\alpha = 2 \times 10^{-5}$ recommended for thrust faults in Anderson and Luco (1983). The equation is applied using both α values.

Here, we present two sets of calculations. The first set directly uses the geodetically derived slip rate for the Quito fault, and four calculations are then performed based on the minimum (4.3 mm/yr) and maximum (5.3 mm/yr) slip-rate bounds, combined with two α values. This calculation implicitly assumes that the fault is locked over the entire seismogenic thickness. The second set accounts for aseismic slip on the Quito fault. Assuming that ε% of the fault surface is creeping, the annual seismic moment rate deficit is

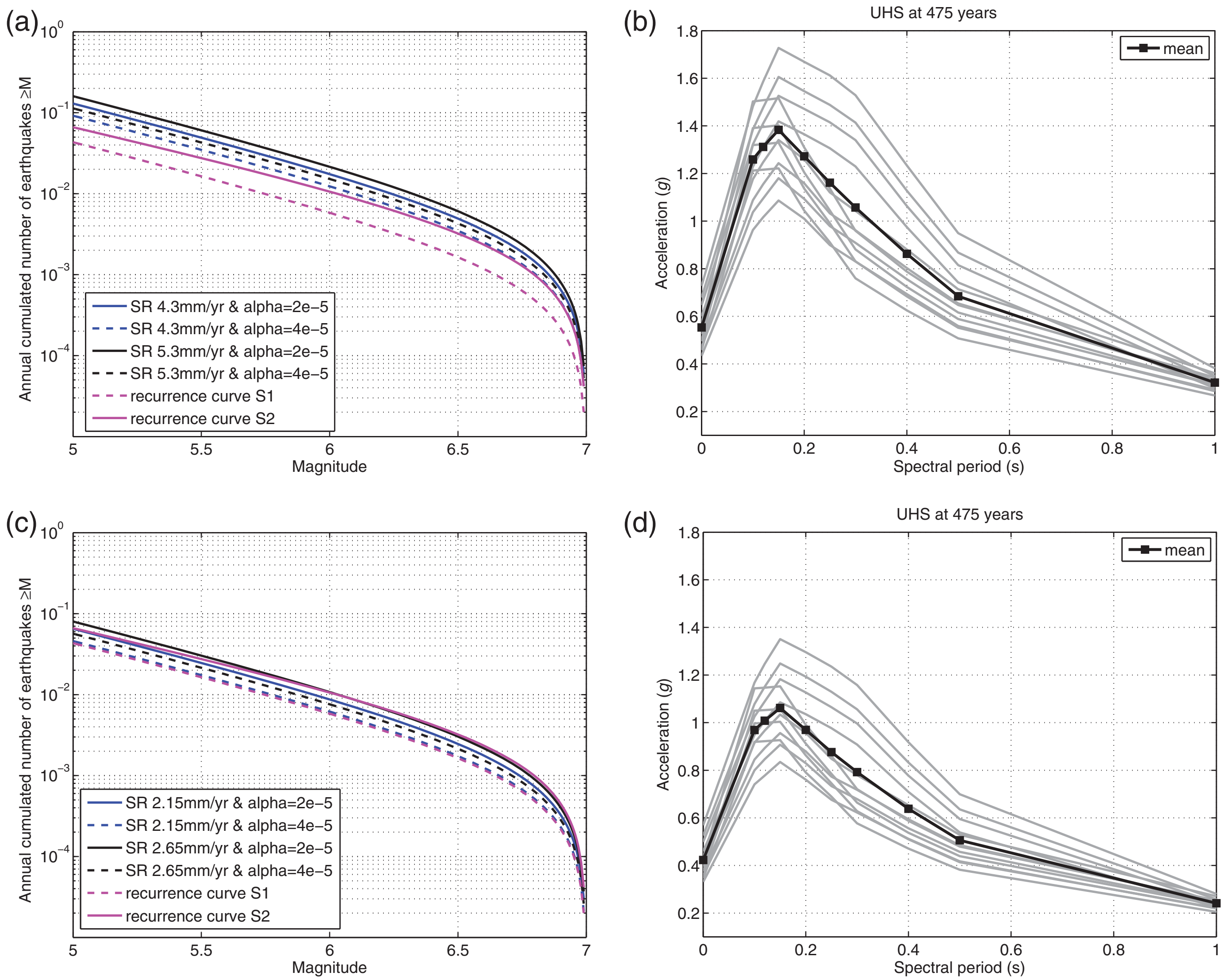

▲ **Figure 8.** (a) Recurrence curves inferred from average slip rates on the Quito fault system (blue and black lines, four optional curves, combination of two slip rates and two α parameters (see Frequency–Magnitude Distributions Based on the Slip Rate and Corresponding Hazard), superimposed on the frequency–magnitude distributions based on earthquake data (S1 resized to the Quito zone area and S2). (b) Uniform hazard spectra in Quito, resulting from the application of the slip rate-based recurrence curves to describe earthquake occurrence in the Quito zone (S2). The 12 uniform hazard spectra correspond to the combinations of four optional recurrence curves and three optional GMPEs (Akkar and Bommer, 2010; Zhao *et al.*, 2006; Boore and Atkinson, 2008). (c) and (d) Same as (a) and (b) with a slip rate reduced by 50% (consistent with a partially locked fault).

$$\dot{M}_0 = \mu A(1 - \varepsilon)S,$$

in which A is the surface of the fault. It is therefore equivalent to divide A or S to obtain the same annual moment rate deficit. Most faults on continents are locked over the whole seismogenic upper crust that is ~15 km. The locking depth of 7 km indicated by the GPS results therefore suggests that ε is close to ~50%. We therefore perform the calculation using 50% of the slip rate ($S/2$) to derive a frequency–magnitude distribution for the case of the partially locked Quito fault.

The first set of calculations provides frequency–magnitude distributions with many more earthquakes than has been observed in the past (Fig. 8a). As a consequence, the resulting recurrence models are predicting higher rates than those inferred from the earthquake catalogs. This trend, that is, modeled rates based on fault slip rates higher than rates based on past seismicity, has been observed in other seismic-hazard studies using GPS strain rates, for example, Mazzotti *et al.* (2011) or in the SHARE project (Woessner *et al.*, 2012). If one divides the measured slip rates into an aseismic and a seismic release, the predicted rates are lower and in agreement with the recurrence inferred from past seismicity (Fig. 8c).

The UHS at 475 years is calculated considering four seismicity models (Quito zone S2, minimum and maximum slip rates, two optional α values) and the three selected crustal GMPEs. Assuming ε equal to 0 (Fig. 8b), the acceleration levels are significantly higher than those relying on the catalog-based recurrence curves (Fig. 7). Accelerations at the PGA vary between $0.43g$ and $0.73g$, at 475 years, with a mean close to $0.55g$. Assuming ε equal to 50% (Fig. 8d), the accelerations are close to those relying on the catalog-based recurrence curves. Accelerations at the PGA vary between $0.32g$ and $0.58g$, with a mean around $0.42g$.

RESTRICTING LARGE EARTHQUAKES TO THE QUITO FAULT AND HANGING-WALL EFFECT

PGA at 475 Years: Profile Perpendicular to the Fault

When modeling the seismicity with areal sources in the probabilistic calculations, the hanging-wall effect cannot be taken into account properly. The city is lying over the hanging wall of the Quito reverse fault system, and in case of a large earthquake below the city, ground motions are expected to be much higher in Quito than in the suburbs at the foot of the hills (footwall, see Fig. 2). There are several past examples of this effect, for example, during the Chi-Chi M_w 7.1 earthquake in Taiwan (Chang *et al.*, 2004). As an attempt to include hanging-wall amplifications, two more GMPEs for crustal earthquakes are included, the Abrahamson and Silva (2008) and Chiou and Youngs (2008) models.

Within the Quito areal zone, all large earthquakes (e.g., $\mathbf{M} \geq 6.0$) are expected to occur on the identified segments of the reverse fault system. Rather than distributing all seismicity rates (M 5–7) homogeneously over the Quito areal zone, an alternative is to distribute the seismicity rates of magnitudes 5–6 over the zone (as background seismicity) and assign the rates of magnitudes 6–7 on the Quito fault plane. To perform this exercise, the simplified fault geometry described in the Frequency–Magnitude Distributions Based on the Slip Rate and Corresponding Hazard section is used. The reverse fault is dipping to the west with an angle of 50°, extending from 3 to 18 km depth (Fig. 9, corresponding to a width around 19–20 km, compatible with an earthquake magnitude around 7.0, Wells and Coppersmith, 1994). There is a significant uncertainty in this geometry, however, the dip and extension in depth are compatible with the distribution of microseismicity and with geomorphological characteristics (relocations of tectonic events by Lamarque [2011] and Font *et al.* [2013], analysis of local microseismicity by Alvarado *et al.* [2014]). Each segment of the fault system has a main compressional and secondary dextral strike-slip component, confirmed by the available focal mechanisms (Segovia and Alvarado, 2009; Alvarado *et al.*, 2014).

At first, calculations are performed applying the frequency–magnitude distribution based on the Quito zone dataset ($b = 0.81$ and rates of $\mathbf{M} \geq 4.5$ equal to 0.11, Fig. 6b). Four GMPEs are applied: Akkar and Bommer (2010), Boore and Atkinson (2008), Abrahamson and Silva (2008), and Chiou and Youngs (2008) (distance measures R_{JB}, R_{JB}, R_{rup}, and R_{rup}, respectively). The PGA obtained at 475 years, for sites located on a profile perpendicular to the fault, is displayed in Figure 10a (profile in Fig. 2). For comparison, accelerations obtained distributing all the seismicity over the areal source zone case are

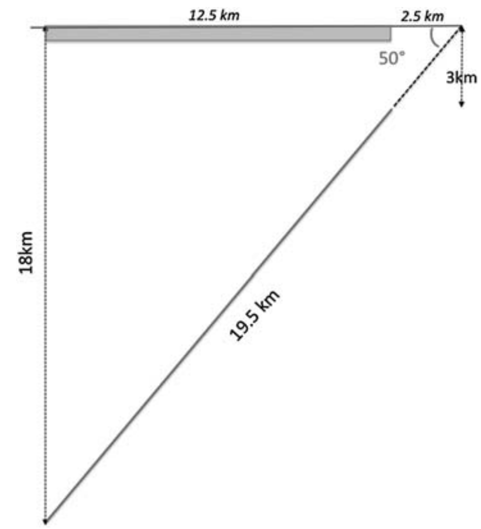

▲ **Figure 9.** Geometry of the simplified fault at depth. Black: dipping fault; gray: surface projection of the fault, as shown by the red dashed line in Figures 10a,b.

also superimposed (see Variability of the Uniform Hazard Spectrum (UHS) section). Concentrating the occurrence of magnitudes 6–7 on the fault plane produces an increase of acceleration levels at sites located above the fault plane ($R_{JB} = 0$). Applying the models Akkar and Bommer (2010) and Boore and Atkinson (2008) (no hanging-wall coefficient) or Chiou and Youngs (2008) (with hanging-wall coefficient) at the sites located above the fault plane results in an increase in accelerations up to 20%–30%. Maximum accelerations of $0.53g$ at 475 years are obtained applying the Akkar and Bommer (2010) ground-motion equation. Applying the equation by Abrahamson and Silva (2008) produces a greater acceleration increase (35% at maximum) with respect to the areal zone case. If using the larger host zone option (S1 zone Quito–Latacunga), the hazard obtained in Quito is higher than when using the smaller Quito host zone. Restricting magnitudes 6–7 to the fault plane (rates proportionated to the Quito zone area) increases accelerations at 475 years by 20%–40% (Fig. 10b), reaching a maximum of $0.68g$ (Akkar and Bommer, 2010 or Abrahamson and Silva, 2008 models).

Scenarios and Hazard Values at 475 Years

The acceleration at 475 years is a threshold, corresponding to the acceleration at the site with a 10% probability of being exceeded at least once over 50 years. All earthquakes included in the model, with low-to-high magnitudes, close or far from the site, with a nonzero probability of producing an acceleration greater than this threshold, contribute to this hazard calculation. It can be interesting, although requires care, to compare these accelerations at 475 years with acceleration levels corresponding to different earthquake scenarios. We believe that such exercises can be helpful to better grasp the meaning of the probabilistic output. The median acceleration to expect in case of a given earthquake on the Quito fault is superimposed on the previous profiles, applying the Abrahamson and Silva

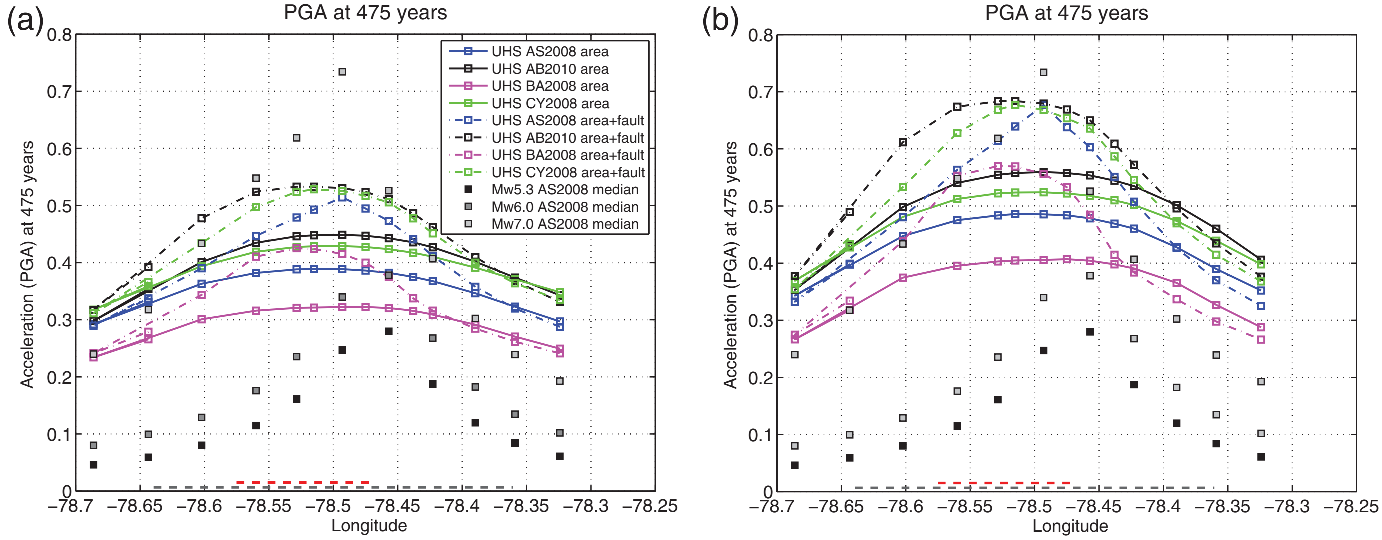

▲ **Figure 10.** PSH in Quito city: PGA acceleration at 475 years, at sites located along a profile perpendicular to the fault (west to east, see Fig. 2); as well as median accelerations predicted for three given earthquake scenarios. Solid line: the frequency–magnitude distribution ($5 \le M_w \le 7$) is homogeneously distributed over the areal zone; dashed line: large magnitudes ($6 \le M_w \le 7$) are restricted to the fault plane. Surface projections of the source zone (dashed black segment) and of the fault plane (red dashed segment) indicated at the bottom. (a) b-value and annual rate of $\mathbf{M} \ge 4.5$ inferred from the seismicity in the Quito zone (S2, $b = 0.81$, $\lambda_{M>4.5} = 0.11$). (b) b-value and annual rate of $\mathbf{M} \ge 4.5$ inferred from the seismicity in the Latacunga–Quito zone (S1, $b = 0.72$, $\lambda_{M>4.5} = 0.15$). Gray squares: median accelerations predicted for M_w 5.3, 6.0, and 7.0, using the GMPE model AS2008. AS2008: Abrahamson and Silva (2008); AB2010: Akkar and Bommer (2010); BA2008: Boore and Atkinson (2008); and CY2008: Chiou and Youngs (2008).

(2008) equation. The accelerations correspond to an earthquake occurring on the segment of the fault intersecting the profile. The smallest magnitude considered is 5.3 (M_w), similar to that of an earthquake that occurred in 1990 on a northern segment of the fault (Pomasqui, 11 August 1990, Fig. 2), which could be repeated anywhere on the fault. Two larger events are considered: an earthquake with M_w 6.0, which probably occurred at least once in the last five centuries (Beauval *et al.*, 2010, 2013), and an earthquake with M_w 7.0 corresponding to the complete rupture of the fault (for which there is evidence of only one, from paleoseismology, 500–1000 years ago, Hibsch *et al.*, 1997). Results displayed in Figure 10a,b show that, whatever the decision on the seismicity model or the GMPE, the acceleration levels at 475 years are greater than the acceleration corresponding to the M_w 5.3 scenario. Considering the worst scenario in our seismicity model, M_w 7.0, the maximum acceleration to expect (if considering only the median) exceeds the maximum acceleration at 475 years, whatever the combination of models chosen.

CONCLUSIONS

In the present study, PSH estimates at 475 years return period for Quito, capital city of Ecuador, show that the crustal host zone is the only source zone that determines the city's hazard levels for such return period. Therefore, the emphasis is put on identifying the uncertainties characterizing the host zone, that is, uncertainties in the recurrence of earthquakes expected in the zone and uncertainties on the ground motions that these earthquakes may produce. As the number of local strong ground motions is still scant, GMPEs are imported from other regions. Rather than sampling a complex logic tree, several plausible models are considered and associated with the corresponding uniform hazard spectra.

Exploring recurrence models for the host zone based on different observations and assumptions, and including three GMPE candidates (Zhao *et al.*, 2006; Boore and Atkinson, 2008; Akkar and Bommer, 2010), we obtain a significant variability on the estimated acceleration at 475 years (site coordinates: −78.51° in longitude and −0.2° in latitude, V_{S30}760 m/s):

- Considering historical earthquake catalogs, and relying on frequency–magnitude distributions where rates for magnitudes 6–7 are extrapolated from statistics of magnitudes 4.5–6.0 mostly in the twentieth century, the acceleration at the PGA varies between 0.28g and 0.55g with a mean value around 0.4g. The results show that both the uncertainties in the GMPE choice and in the seismicity model are responsible for this variability.
- Considering slip rates inferred from geodetic measurements across the Quito fault system, and assuming that most of the deformation occurs seismically (conservative hypothesis), leads to a much greater range of accelerations, 0.43g–0.73g for the PGA (with a mean of 0.55g).
- Considering slip rates inferred from geodetic measurements, and assuming that 50% only of the deformation is released in earthquakes (partially locked fault, model based on 15 years of GPS data), leads to a range of accelerations 0.32g–0.58g for the PGA, with a mean of 0.42g.

These accelerations are in agreement with the catalog-based hazard estimates.

- Restricting the occurrence of magnitudes 6–7 to the Quito fault (a simplified geometry), applying the three initial GMPEs (Akkar and Bommer, 2010; Zhao *et al.*, 2006; Boore and Atkinson, 2008) or GMPEs including a hanging-wall coefficient (Abrahamson and Silva, 2008; Chiou and Youngs, 2008), increases the hazard by 20%–40% at sites located above the fault plane (range $0.42g$–$0.68g$ at the considered site). Strong hypotheses are required to define a simple fault plane and to define the recurrence of earthquakes on this fault plane; therefore, these results must be taken with great caution. However, they demonstrate that taking into account faults in hazard calculations can have a major impact.

Modeling the recurrence based on the past earthquake catalog, and relying on an areal source zone model, gives a mean value around $0.4g$ for the PGA at 475 years in Quito. This mean value is for a site on rock, and site effects need to be further taken into account. These results are in accordance with the acceleration level recently adopted by the new Ecuadorian Building Code (MIDUVI-CCQ, 2011). The seismic provisions of this Building Code are based on our 2011 national PSH map at rock, based on a single best-estimate model (no logic tree and no exploration of uncertainties). Nonetheless, based on various exercises, we show that if taking into account the fault itself in the hazard calculations, much higher values can be obtained for sites located above the fault. Interdisciplinary studies must be pursued to better understand paleoseismicity and fault kinematics around Quito. Soon there will be enough recordings available from the recently installed strong-motion stations, so that imported GMPEs can be tested to refine the selection. Future research should also focus on understanding better how to include source–site geometry effects such as the hanging wall, as these effects will certainly have direct consequences on the damage distribution in case of a large destructive earthquake.

ACKNOWLEDGMENTS

The authors thank Editor Zhigang Peng and two anonymous reviewers for their helpful and constructive reviews of the manuscript, as well as Brian E. Tucker (Geohazards International) for careful proofreading of the manuscript and for improving the English. In addition, we thank Fabrice Cotton for insightful comments on the manuscript, which led to significant improvements. This work was partially supported by the laboratory ISTerre, by the Agence Nationale de la Recherche through the project Andes du Nord (Contract Number ANR-07-BLAN-143-01), and by the Institut de Recherche pour le Développement (IRD). Hugo Yepes' stays in Grenoble also benefited from a LabEx OSUG@2020 Grant Number (ANR10 LABX56), as well as from the MEEES Erasmus Mundus program (www.meees.org/; last accessed October 2014). On the Ecuadorian side, additional support was available from the Secretaría Nacional de Educación Superior, Ciencia y Tecnología SENESCYT (LAE-5 y Proyecto PIN_08-EPNGEO-00001). This work has been carried out in the frame of the Joint International Laboratory "Seismes & Volcans dans les Andes du Nord" (IRD LMI SVAN). Finally, we are grateful to the Global Earthquake Model (GEM) Modeling Facility for constant support on the handling of the OpenQuake software since 2010 (www.globalquakemodel.org; last accessed October 2014).

REFERENCES

Abrahamson, N., and W. Silva (2008). Summary of the Abrahamson & Silva NGA ground-motion relations, *Earthq. Spectra* **24,** no. 1, 67–97.

Akkar, S., and J. J. Bommer (2010). Empirical equations for the prediction of PGA, PGV and spectral accelerations in Europe, the Mediterranean and the Middle East, *Seismol. Res. Lett.* **81,** no. 2, 195–206.

Anderson, J. G., and J. E. Luco (1983). Consequences of slip rate constraints on earthquake occurrence relations, *Bull. Seismol. Soc. Am.* **73,** no. 2, 471–496.

Alvarado, A. (2012). Néotectonique et cinématique de la déformation continentale en Equateur, *Thèse de doctorat (Ph.D.)*, Université de Grenoble, France, 259 pp.

Alvarado, A., L. Audin, J. M. Nocquet, M. Segovia, Y. Font, G. Lamarque, H. Yepes, P. Mothes, F. Rolandone, and P. Jarrin (2014). Active tectonics in Quito, Ecuador, assessed by geomorphological studies, GPS data, and crustal seismicity, *Tectonics*, doi: 10.1002/2012TC003224.

Arango, M., F. Strasser, J. Bommer, J. Cepeda, R. Boroschek, D. Hernandez, and H. Tavera (2012). An evaluation of the applicability of current ground-motion models to the south and central American subduction zones, *Bull. Seismol. Soc. Am.* **102,** 143–168.

Beauval, C., and O. Scotti (2003). Mapping b-values in France using two different magnitude ranges: Possible non power-law behavior, *Geophys. Res. Lett.* **30,** no. 17, 1892, doi: 10.1029/2003GL017576.

Beauval, C., F. Cotton, N. Abrahamson, N. Theodulidis, E. Delavaud, L. Rodriguez, F. Scherbaum, and A. Haendel (2012). Regional differences in subduction ground motions, *World Conference on Earthquake Engineering*, Lisboa, Portugal, 24–28 September, 10 pp.

Beauval, C., H. Tasan, A. Laurendeau, E. Delavaud, F. Cotton, Ph. Guéguen, and N. Kuehn (2012). On the testing of ground-motion prediction equations against small magnitude data, *Bull. Seismol. Soc. Am.* **102,** no. 5, 1994–2007.

Beauval, C., H. Yepes, W. Bakun, J. Egred, A. Alvarado, and J.-C. Singaucho (2010). Locations and magnitudes of historical earthquakes in the Sierra of Ecuador (1587–1996), *Geophys. J. Int.*, doi: 10.1111/j.1365-246X.2010.04569.x.

Beauval, C., H. Yepes, P. Palacios, M. Segovia, A. Alvarado, Y. Font, J. Aguilar, L. Troncoso, and S. Vaca (2013). An earthquake catalog for seismic hazard assessment in Ecuador, *Bull. Seismol. Soc. Am.* **103,** 773–786, doi: 10.1785/0120120270.

Boore, D., and G. Atkinson (2008). Ground motion prediction equations for the average horizontal component of PGA, PGV, and 5%-damped PSA at spectral periods between 0.01 s and 10.0 s, *Earthq. Spectra* **24,** 99–138.

Bungum, H. (2007). Numerical modelling of fault activities. *Comput. Geosci.* **33,** 808–820.

Champenois, J., L. Audin, S. Baize, J.-M. Nocquet, and A. Alvarado (2013). Interseismic deformations along Ecuador active fault systems: Contribution of space-borne SAR interferometry, *AGU Meeting of the Americas*, Mexico, Cancun, 14–17 May.

Chang, T.-Y., F. Cotton, Y.-B. Tsai, and J. Angelier (2004). Quantification of hanging-wall effects on ground motion: some insights from the 1999 Chi-Chi earthquake, *Bull. Seismol. Soc. Am.* **94,** no. 6, 2186–2197.

Chatelain, J. L., B. Tucker, B. Guillier, F. Kaneko, H. Yepes, F. Fernandez, J. Valverde, G. Hoefer, M. Souris, E. Dupérier, T. Yamada, G. Bustamante, and C. Villacis (1999). Earthquake risk management pilot project in Quito, Ecuador, *Geojournal* **49,** 185–196.

Chiou, B. S.-J., and R. R. Youngs (2008). An NGA model for the average horizontal component of peak ground motion and response spectra, *Earthq. Spectra* **24,** 173–215.

Crowley, H., D. Monelli, M. Pagani, V. Silva, and G. Weatherill (2013). Hands-on-instructions on the different types of calculations you can carry out with the OpenQuake Engine Software, *Openquake Engine, User Instruction Manual, Version 1.0.0*, Global Earthquake Model, 154 pp.

Delavaud, E., F. Cotton, S. Akkar, F. Scherbaum, L. Danciu, C. Beauval, S. Drouet, J. Douglas, R. Basili, M. A. Sandikkaya, M. Segou, E. Faccioli, and N. Theodoulidis (2012). Toward a ground-motion logic tree for probabilistic seismic hazard assessment in Europe, *J. Seismol.*, doi: 10.1007/s10950-012-9281-z.

Ego, J., and M. Sebrier (1996). The Ecuadorian inter-Andean valley: A major and complex restraining bend an compressive graben since late Miocene time, *Annales Tectonicae* **X,** 31–59.

Egred, J. (2009). Catalogo de terremotos del Ecuador 1541–2009, Escuela Politecnica Nacional, Instituto Geofisico, *Internal Report*.

Font, Y., S. Segovia, S. Vaca, and T. Theunissen (2013). Seismicity pattern along the Ecuadorian subduction zone: Newconstrains from earthquake location in a 3D a priori velocity model, *Geophys. J. Int.*, doi: 10.1093/gji/ggs083.

Gutenberg, B., and F. Richter (1944). Frequency of earthquakes in California, *Bull. Seismol. Soc. Am.* **34,** 185–188.

Hibsch, C., A. Alvarado, H. Yepes, V. H. Perez, and M. Sébrier (1997). Holocene liquefaction and soft-sediment deformation in Quito (Ecuador): A paleoseismic history recorded in lacustrine sediments, *J. Geodyn.* **24,** 259–280.

Kanamori, H., and D. L. Anderson (1975). Theoretical basis of some empirical relations in seismology, *Bull. Seismol. Soc. Am.* **65,** 1073–1095.

Lamarque, G. (2011). Analyse méthodologique pour la localisation de séismes dans la zone de Quito et corrélation avec les failles actives, Mémoire M1, Université de Nice Sophia-Antipolis, 33 pp.

Lavenu, A., T. Winter, and F. Dávila (1995). A Pliocene-Quaternary compressional 899 basin in the Interandean depression, central Ecuador, *Geophys. J. Int.* **121,** 279–300.

Leonard, M. (2010). Earthquake fault scaling: Self-consistent relating of rupture length, width, average displacement, and moment release, *Bull. Seismol. Soc. Am.* **100,** no. 5A, 1971–1988, doi: 10.1785/0120090189.

Mazzotti, S., L. J. Leonard, J. F. Cassidy, G. C. Rogers, and S. Halchuk (2011). Seismic hazard in western Canada from GPS strain rates versus earthquake catalog, *J. Geophys. Res.* **116** , B12310 doi: 10.1029/2011JB008213.

Medvedev, S. V., W. Sponheuer, and V. Karnik (1963). Seismiche Scala, Inst fiir Bodendynamik und Erdbebenforshung, Jena, 6 pp.

MIDUVI-CCQ (2011). Norma Ecuatoriana de la Construcción NEC-11, *Cap. 2: Peligro Sísmico, y Requisitos de Diseño Sismo Resistente*, Cámara de la Construcción de Quito, http://www.normaconstruccion.ec/ (last accessed October 2014).

Nocquet, J.-M., J. C. Villegas-Lanza, M. Chlieh, P. A. Mothes, F. Rolandone, P. Jarrin, D. Cisneros, A. Alvarado, L. Audin, F. Bondoux, X. Martin, Y. Font, M. Régnier, M. Vallée, T. Tran, C. Beauval, J. M. Maguiña Mendoza, W. Martinez, H. Tavera, and H. Yepes (2014). Continental deformation and creeping subduction in the Northern Andes, *Nature Geosci.* **7,** 287–291.

Pagani, M., D. Monelli, G. Weatherill, L. Danciu, H. Crowley, V. Silva, P. Henshaw, L. Butler, M. Nastasi, L. Panzeri, M. Simionato, and D. Vigano (2014). OpenQuake-engine: An open hazard (and risk) software for the gobal earthquake model, *Seismol. Res. Lett.* **85,** 692–702.

Pino, D., and H. Yepes (1990). « Apuntes para una historia sismica de Quito. Centro Historico de Quito. Problematica y perspectivas », Direccion de planificaion, Ilustre Municipio de Quito, Ecuador.

Segovia, M., and A. Alvarado (2009). Breve análisis de la sismicidad y del campo de esfuerzos en el Ecuador, in *Geología y geofísica marina y terrestre del Ecuador: Desde la costa continental hasta las Islas Galápagos*, J.-Y. Collot, V. Sallares, and N. Pazmiño (Editors), Comision Nacional Del Derecho del Mar (CNDM), Guayaquil-Ecuador, 131–150, ISBN: 978-9978-92-737-3.

Soulas, J.-P., A. Egüez, H. Yepes, and V. H. Perez (1991). Tectónica activa y riesgo sísmico en los Andes Ecuatorianos y en el extremo Sur de Colombia, *Boletín Geológico Ecuatoriano* **2,** no. 1, 3–11.

Strasser, F., M. C. Arango, and J. J. Bommer (2010). Scaling of the source dimensions of interface and intraslab subduction-zone earthquakes with moment magnitude, *Seismol. Res. Lett.* **81,** no. 6, 941–950.

Weichert, D. H. (1980). Estimation of the earthquake recurrence parameters for unequal observation periods for different magnitudes, *Bull. Seismol. Soc. Am.* **70,** no. 4, 1337–1346.

Wells, D. L., and K. J. Coppersmith (1994). New empirical relationships among magnitude, rupture length, rupture width, rupture area, and surface displacement, *Bull. Seismol. Soc. Am.* **84,** no. 4, 974–1002.

Woessner, J., D. Giardini, and The SHARE Consortium (2012). Seismic hazard estimates for the Euro-Mediterranean region: A community-based probabilistic seismic hazard assessment, *Proceedings of the 15th World Conference of Earthquake Engineering*, Lisbon, Portugal, 24–28 September, Paper No. 4337.

Youngs, R., and K. Coppersmith (1985). Implications of fault slip rates and earthquake recurrence models to probabilistic seismic hazard estimates, *Bull. Seismol. Soc. Am.* **75,** 939–964.

Youngs, R. R., S. J. Chiou, W. J. Silva, and J. R. Humphrey (1997). Strong ground motion attenuation relationships for subduction zone earthquakes, *Seismol. Res. Lett.* **68,** no. 1, 58–73.

Zhao, J. X., J. Zhang, A. Asano, Y. Ohno, T. Oouchi, T. Takahashi, H. Ogawa, K. Irikura, H. K. Thio, P. G. Somerville, Y. Fukushima, and Y. Fukushima (2006). Attenuation relations of strong ground motion in Japan using site classifications based on predominant period, *Bull. Seismol. Soc. Am.* **96,** no. 3, 898–913.

Céline Beauval
Laurence Audin
ISTerre
Univ. Grenoble Alpes-CNRS-IRD
F-38041 Grenoble, France
celine.beauval@ujf-grenoble.fr

Hugo Yepes
Alexandra Alvarado
Instituto Geofisico
Escuela Politécnica Nacional
Ladrón de Guevara
2759 Quito, Ecuador

Jean-Mathieu Nocquet
Geoazur
IRD, Université de Nice Sophia-Antipolis
Observatoire de la Côte d'Azur, CNRS
250, Rue A. Einstein
06560 Valbonne, France

Damiano Monelli
Laurentiu Danciu
GEM Hazard Team
SED-ETHZ
Sonneggstrasse 5
8092 Zurich, Switzerland

Published Online 22 October 2014

[1] Also at ISTerre, Univ. Grenoble Alpes-CNRS-IRD, F-38041 Grenoble, France.